

Technical Article

- Experimental Simulation on Sodium Leak through Roof Slab-LRP Gap of PFBR under HCDA

Young Officer's Forum

- In-Situ Detection of Early Corrosion of Ferritic Cr-Mo Steel in Aqueous Solutions of different Anions using Laser Raman Spectroscopy

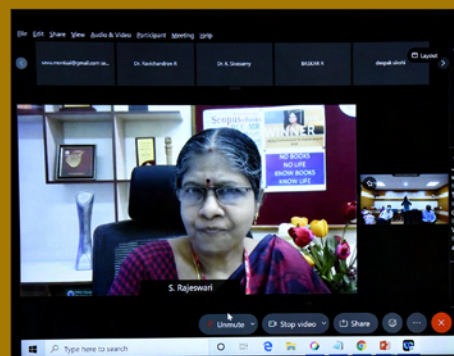
Young Researcher's Forum

- In-house Development of High-Temperature Drop Calorimeter and Measurement of Enthalpy Increment of Magnesium Oxide

Events

Awards, Honours and Recognitions

Back Cover: Bio-diversity @ DAE Campus, Kalpakkam



From the Editor's Desk

Dear Reader

It is my pleasant privilege to forward the latest issue of IGC Newsletter (Volume 129, July 2021, Issue 3). I thank my team for their timely inputs, cooperation, and support in bringing out this issue.

The digital copy is published through the websites <http://vaigai> and <http://www.igcar.gov.in>. Additionally, on the Vaigai website, the flip copy of the Newsletter is available.

The technical article is on "Experimental Simulation on Sodium Leak through Roof Slab-LRP Gap of PFBR under HCDA" The article is contributed by Shri S. Athmalingam and his Colleagues from the Safety, Quality & Resource Management Group.

Young Officer's Forum features an article by Mr. C. Thinaharan, Metallurgy & Materials Group. Shri Supratim Mukherjee of Materials Chemistry & Metal Fuel Cycle Group, IGCAR has contributed Young Researcher's Forum article in this issue.

Further, we have included highlights of our colleagues awards, honors, and recognitions in this issue.

The back cover of the IGC Newsletter has male and female parakeets this time. Our photographer documented them in 2017 in the tree next to DPS Stores, IGCAR. We find a rise in their numbers in recent years within our campus.

The Editorial Committee would like to thank all the contributors. We look forward to receiving constructive suggestions from readers towards improving the IGC Newsletter content.

Use Face Mask. Maintain Social Distance to break the chain. Vaccinate. Stay Safe.

With best wishes and regards

S. Rajeswari
Chairman, Editorial Committee, IGC Newsletter and
Head, Scientific Information Resource Division, IGCAR

Experimental Simulation on Sodium Leak through Roof Slab-LRP Gap of PFBR under HCDA

Prototype Fast Breeder Reactor (PFBR) consists of large sodium inventory (~1150 t) in the main vessel. During normal operating conditions, no sodium leak is envisaged into Reactor Containment Building (RCB) from the main vessel. However, in case of a hypothetical core disruptive accident (HCDA), due to failure of mechanical seals, sodium may leak into the RCB through LRP (large rotating plug), SRP (small rotating plug) penetrations in roof slab. Theoretically, sodium of ~102 kg may get ejected through roof slab-LRP gap (path 1 in Figure 1) and will spread over an area of 75 m². Roof slab openings in PFBR are packed with Rockwool insulation and are covered with a carbon steel plate on top.

During HCDA, the ejected sodium interacts with constituents and oxygen available in the insulation. The top cover plate reduces oxygen ingress into leaked sodium and minimizes the amount of sodium combustion. Energy released from sodium combustion may raise the temperature of the roof slab plate and consequently, pressure in RCB. As the combustion of radioactive sodium determines the source term in RCB, the actual prediction of ejected sodium quantity and its combustion are very important for source term assessment. Hence, an experimental study has been taken up at SED, using a scaled geometric model of roof slab-LRP gap to determine the amount of sodium release and its potential to undergo combustion. A scale down sector model

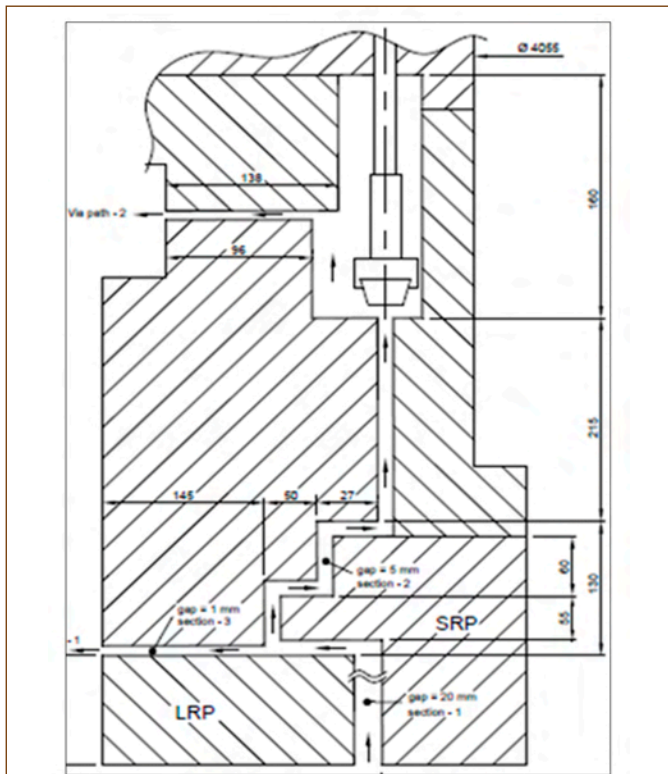


Figure 1: Leak paths in roof slab TSP

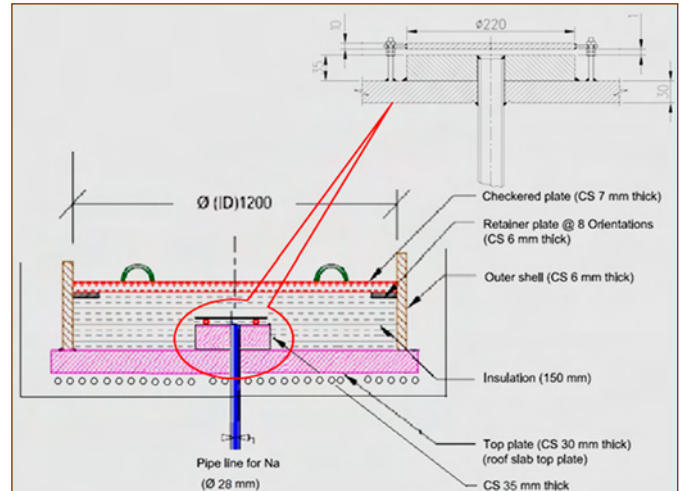


Figure 2: Simulation of roof slab-LRP leak path

(Figure 2) having an area of 1.13 m² area has been considered and accordingly, a leak of 1.56 kg in 0.6 s is simulated.

Experimental Setup

The experimental setup consists of a carbon steel structure simulating PFBR roof slab-LRP leak path housed in a cylindrical test chamber of ~20 m³ volume as shown in Figure 1. The setup is fabricated by fixing two CS plates of 220 mm diameter each, at a gap of 1 mm over a CS plate of 1.2 m diameter at bottom as shown Figure 3. The bottom plate is covered with thermal insulation upto a height of 150 mm. The setup is integrated to a sodium system for upward ejection simulating sodium slug impact on bottom of the roof slab during HCDA. The sodium system consists of a sodium vessel of 6 litre volume, transfer line and argon cover gas system for maintaining required gas pressure.



Figure 3: Simulation of roof slab-LRP leak path

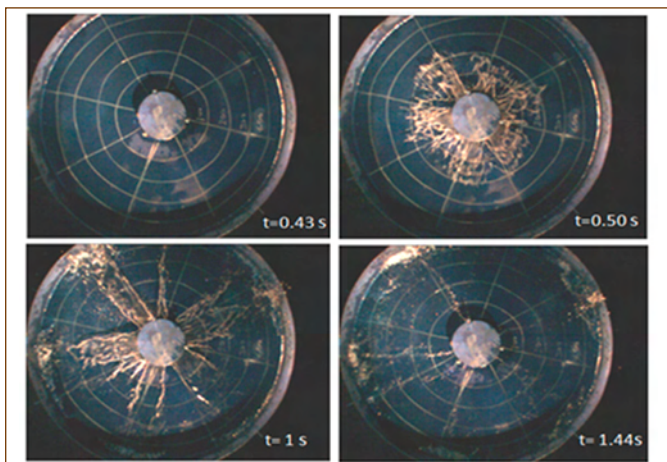


Figure 4: Ejection of water through 1 mm gap

Sodium vessel is erected in a pit beneath the cylindrical chamber and sodium transfer line connects at the centre of the bottom plate through a pneumatically operated bellow sealed valve (PBSV). The sodium system and top plate are provided with surface heaters required for preheating to 550 °C and 110 °C respectively. Solenoid valves are provided in the argon circuit for pressurization of the sodium system. A timer circuit was integrated to the PBSV for controlling the sodium ejection time to 0.6 s.

Preliminary experiments with water

Preliminary experiments were carried out with water for determining the exact pressure and release time settings required for ejecting 1.56 kg of sodium through 1 mm gap within 0.6 s at a flow rate of 2.5 kg/s. From the velocity data obtained using high speed video images at various pressures from 1.7 to 3 bar and based on head loss calculations, the driving pressure required for ejection of sodium was fixed at 2.46 bar. Images of water ejection at various time intervals are shown in Figure 4.

Experiments with Sodium

About 3 kg of pure sodium obtained from glove box maintained at 15 ppm oxygen concentration was loaded in the sodium vessel. Sodium was preheated to 550 °C, while top plate (roof slab setup) was heated to 110 °C. Liquid sodium was ejected for a time span of 0.6 s under a driving pressure of 2.46 bar through 1 mm gap. During the experiment, video imaging using high speed camera



Figure 5: Packing of insulation around leak path

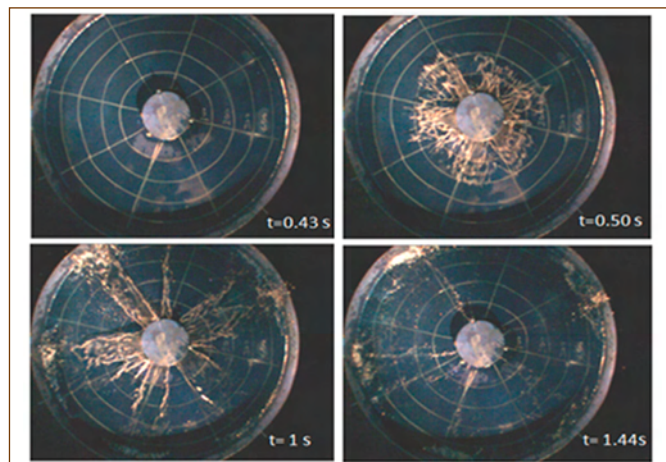


Figure 6: Arrangement of thermocouples

and temperature monitoring at critical locations were carried out.

Sodium experiments were conducted at three configurations

1. Roof slab-LRP gap of 1 mm surrounded by tight packing of insulation
2. With a 10 mm radial gap between the leak path and insulation
3. Without insulation around the leak path

1. Leak path tightly packed with insulation

In this configuration, three layers of 50 mm thick rock wool insulation was arranged around the leak path as shown in Figure 5. About 53 thermocouples (TCs) were positioned at various locations of the top plate and insulation for monitoring the temperatures during sodium ejection.

The arrangement of thermocouples along with TC trees is shown in Figure 6. Each TC tree contains 5 TCs for measuring temperatures at various depths.

During sodium ejection, no spillage of sodium outside the top plate or sodium fire was observed in the test chamber (Figure 7).

Thermocouples provided on the baffle plate indicated a temperature raise of about 25 °C from the background values of 110 °C within 30 s immediately after the release of sodium as shown in Figure 8. TCs at other locations indicated very insignificant temperature rise indicating asymmetric sodium

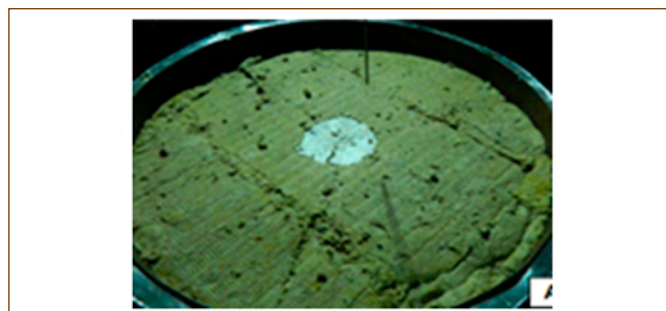


Figure 7: Ejected sodium through 1 mm leak path

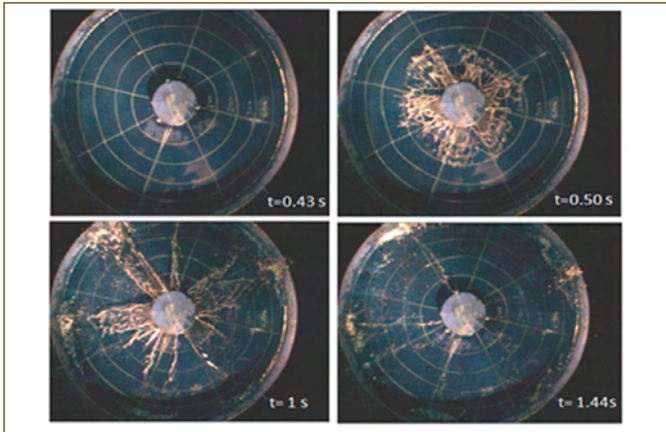


Figure 8: Temperature of ejected sodium



Figure 10: Ejected sodium without insulation

ejection in each direction. Within one mm gap, about 30 g of sodium was trapped. The total sodium ejected out was found to be ~ 290 g. This reduction in ejected quantity could be attributed to the tight packing of insulation and significant heat loss from sodium to the structure during ejection.

2. Radial gap of 10 mm between insulation and leak path

In this case, a cylindrical pipe segment of 250 mm length top was attached to the baffle plate to simulate external cylindrical geometry of LRP. Heaters are provided inside the pipe to maintain its temperature at 110 °C. The insulation was packed at a radial gap of 10 mm from the leak path to simulate the realistic conditions. Few additional thermocouples were arranged for temperature measurements at the gap areas. In this configuration, no sodium spillage was observed in the test chamber. TCs positioned at the gap areas indicated a temperature rise of 40 °C in all directions indicating sodium leak in all directions. The amount of sodium ejected was about 286 g and the majority of sodium was observed within the 10 mm radial gap (Figure 9).

3. No insulation on the cover plate

In this configuration, no thermal insulation was placed around the leak path and on the top plate. However, the temperature of the top plate was maintained at 110 °C. Similar to the previous two configurations, no sodium ejection or fire was observed in the test chamber. Sodium ejection was observed in all directions. Immediately after sodium release, about 20 °C temperature rise



Figure 9: Ejected sodium around the radial gap of leak path

was observed near the leak path on the cover plate at a radial distance of 10 mm. About 290 g of sodium got collected during the sodium ejection on the cover plate (Figure 10).

Results and Discussion

The reason for such low temperatures of ejected sodium could be attributed to significant convective heat transfer that takes place between the flowing sodium and CS cover plates (1 mm gap) with a huge heat transfer area. Moreover, the mass of CS cover plate (14 kg) is higher than the amount of sodium ejected resulting in a drop in sodium temperature. This might have led to increased flow resistance resulting in less quantity of sodium.

An experimental study has been taken up to estimate the amount of sodium leakage through roof slab and LRP gap of PFBR during HCDA scenario. A carbon steel roof slab model with 1 mm leak path and associated sodium & argon systems were installed. Experiments were carried out at three configurations of leak ejection such as (i) with tight packing of thermal insulation surrounding the leak path (ii) with a gap of 10 mm between leak path and thermal insulation and (iii) without any insulation surrounding the leak path. In all the cases, sodium at 550 °C was ejected through the gap under a pressure of 2.5 bar for 0.6 s. Temperatures recorded at various locations indicated that sodium got significantly cooled during the passage through 1 mm gap between baffle plate and CS cover plate of roof slab structure. The maximum temperature of sodium measured at the exit of the leak path was about 144 °C. In all the experiments, the amount of sodium that was ejected onto the roof slab structure was ~ 290 g. The experimental results indicated that the actual amount of sodium ejected out through the 1 mm gap is always less than the numerically predicted value. The temperature of sodium ejected was also very low compared with the theoretical value. Hence, during HCDA, no significant sodium combustion of ejected sodium is anticipated.

Reported by

*Shri S. Athmalingam and his Colleagues
Safety, Quality & Resource Management Group*

Young Officer's FORUM



Mr. C. Thinaharan is working as a Technical Officer 'D' at the Corrosion Science and Technology Division, Indira Gandhi Centre for Atomic Research. He acquired B. Sc. and M.Sc (Chemistry) degrees from M. S. University, Tirunelveli and Annamalai University, Chidambaram. His research interests include corrosion product analysis of various ferritic and austenitic steels structural materials, using Raman spectroscopy and X-ray photoelectron spectroscopy. He has authored/co-authored 32 peer reviewed research articles in international journals.

In-Situ Detection of Early Corrosion of Ferritic Cr-Mo Steel in Aqueous Solutions of different Anions using Laser Raman Spectroscopy

Ferritic Cr-Mo steels are widely used as structural materials in chemical, petroleum processing and power generation industries, due to their favorable creep, toughness and corrosion resistance properties at elevated temperature. Particularly, the modified 9Cr-1Mo steel is one of the important structural materials extensively used for crude heater tubes in refineries and steam generator tubes in nuclear and thermal power plants due to its resistance to stress corrosion cracking and creep at elevated temperatures, together with other properties like low thermal expansion coefficient and high thermal conductivity. Ferritic Cr-Mo steels are used as boiler water tubes, steam super-heater elements and chemical plant reformer tubes for heat exchanger applications. In addition to that,

modified 9Cr-1Mo steel is also used in the pressure vessel of high-temperature gas-cooled reactors used for hydrogen production. For the fabrication of components, these materials are often stored in coastal regions where marine aerosols generated by ocean waves can promote chloride-induced pitting corrosion. Further, in some cases, during hydrostatic testing, these materials are exposed to fresh water where they are prone to chloride induced corrosion attack. In-situ characterization of corrosion products of the modified 9Cr-1Mo steel under naturally immersed conditions without application of applied potential in aqueous environments with different pH and corrosive anions like chloride and sulphate has not been reported so far. Since electrochemical perturbations can accelerate corrosion kinetics, and allow oxidation of most of the elements present in the alloy during applied anodic potential, in-situ investigation under different natural corroding conditions is necessary to obtain insights into the early corrosion phenomena for the development of suitable inhibitors or corrosion mitigation strategies. Further, an aqueous media can shield the corrosion products from phase transformation due to exposed to air/laser-induced heating. This study was aimed at probing early corrosion of modified 9Cr-1Mo steel immersed in four different aqueous solutions of acidic sulphate, neutral chloride, fresh water and alkaline using in-situ laser Raman spectroscopy (LRS) and the characterization of the surfaces by X-ray photoelectron spectroscopy (XPS). In-situ Raman spectra were acquired at different immersion times of 5, 20, 40, 60 and 120 h. The initial corrosion products, their stability and transformations on the surface of the modified 9Cr-1Mo steel are compared with that of carbon steel (CS) corrosion under identical conditions to understand the role of alloying elements.

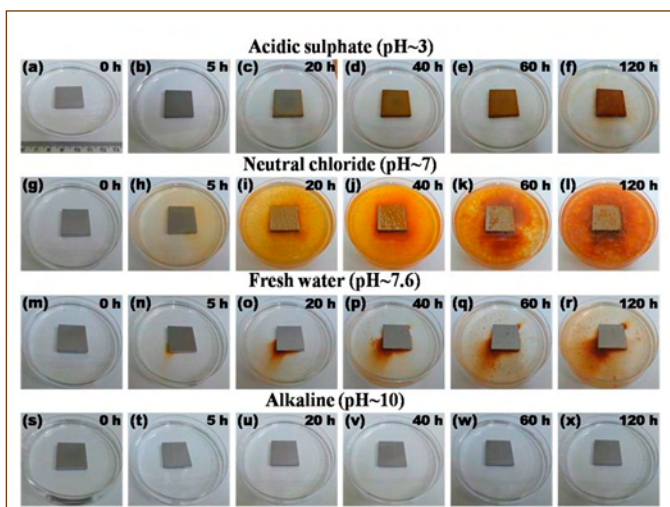


Figure 1: Photographs of bare modified 9Cr-1Mo specimens at different immersion times of 0, 5, 20, 40, 60 and 120 h, in acidic sulphate (a-f), neutral chloride (g-l), fresh water (m-r) and alkaline (s-x) solutions.

The digital photographs of bare modified 9Cr-1Mo steel specimens in aqueous corrosive media at various immersion times of 0, 5, 20, 40, 60 and 120 h are shown in Figure 1. Uniform, pitting, and crevice corrosion was observed in acidic sulphate, neutral chloride, and freshwater environments, respectively. The clean surface was observed throughout the immersion times without any corrosion attack in alkaline solution, suggests that the native film remains on the surface before immersion, its stability is a function of the solution chemistry.

In-situ Raman spectra were acquired on the surface of modified 9Cr-1Mo steel specimen immersed in aqueous corrosive media, up to 120 h. The Raman spectra obtained in acidic sulphate solution are shown in Figure 2, and the wave number corresponding to the Raman peaks are listed in Table. 1.

The spectrum at 5 h exposure time shows a small broad hump at wave number of 667 cm^{-1} (Figure 2b) corresponding to magnetite phase. The peak intensity corresponding to magnetite phase was increased with exposure time to 20 h. Additionally, two low-frequency peaks at 253 and 385 cm^{-1} , were appeared at 20 h immersion time, which are the characteristic peaks of lepidocrocite phase ($\gamma\text{-FeOOH}$). Further, the increase in exposure times to 40 and 60 h, the peak intensities increased, indicating the increased amount of lepidocrocite and the additional broad hump with a low-intensity peak at 719 cm^{-1} due to the formation of maghemite ($\gamma\text{-Fe}_2\text{O}_3$). However, at 120 h exposure time, several black spots together

with reddish-brown color deposits were observed, indicating the formation of different corrosion products. Raman spectra acquired from two regions, namely region 1 (reddish-brown) and region 2 (black), are shown in Figure 2c. The spectrum acquired from region 1, showed the Raman peaks at $220, 256, 314, 350, 382, 531$ and 652 cm^{-1} corresponding to lepidocrocite. The new sets of the peaks at $301, 394, 415, 483$ and 552 cm^{-1} corresponding to goethite phase ($\alpha\text{-FeOOH}$) along with lepidocrocite bands, suggest the transformation of lepidocrocite to goethite. Similarly, the spectrum of region 2 showed both lepidocrocite and goethite peaks with varying intensity ratio. However, peaks corresponding to the goethite phase are predominant, in the black regions. Similarly the in-situ Raman spectra were obtained in neutral chloride and fresh water solutions and the peak positions corresponding to corrosion products are presented in Table. 1.

The corrosion rates of modified 9Cr-1Mo steel at room temperature in acidic sulphate (pH~3), neutral chloride (pH~7), fresh water (pH~7.6) and alkaline (pH~10) were calculated by weight loss method for 120 h exposure. The highest corrosion rate of 0.0827 mm/y was observed in neutral chloride solution as compared to other corrosive media. In alkaline solution, a negligible corrosion rate of 0.0017 mm/y was obtained. With respect to alkaline solution, the order of increase in corrosion rate was approximately ~ 50, 20 and 5.5 times respectively, in neutral chloride, acidic sulphate and fresh water media. As shown in Figures 1g-l, visual examination

Table 1 : Raman peak positions of rust phases in the region $200\text{--}850\text{ cm}^{-1}$ recorded with a 633 nm laser excitation source during the immersion in corrosive media.

Immersion time (h)	Compound	Acidic sulphate (pH~3) Peak positions (cm^{-1})	Neutral chloride (pH~7) Peak positions (cm^{-1})	Fresh water (pH~7.6) Peak positions (cm^{-1})
5	Fe_3O_4	667	668	-----
	$\gamma\text{-FeOOH}$	-----	253, 382	-----
20	Fe_3O_4	668	-----	-----
	$\gamma\text{-FeOOH}$	253, 384	253, 381, 648	250, 380, 650
	$\gamma\text{-Fe}_2\text{O}_3$	-----	-----	719
40	$\gamma\text{-FeOOH}$	222, 254, 308, 382, 532, 649	254, 382, 531, 649	250, 381, 647
	$\gamma\text{-Fe}_2\text{O}_3$	718	-----	719
60	Fe_3O_4	-----	667	-----
	$\gamma\text{-FeOOH}$	223, 254, 309, 352, 383, 531, 650	221, 254, 309, 348, 382, 530	222, 251, 308, 350, 382, 528, 648
	$\gamma\text{-Fe}_2\text{O}_3$	719	-----	719
120 (Region 1)	$\gamma\text{-FeOOH}$	220, 255, 314, 351, 382, 531, 653	220, 254, 312, 350, 381, 530, 648	222, 254, 312, 349, 382, 530, 649
	$\alpha\text{-FeOOH}$	302, 394, 403, 483, 557	-----	-----
120 (Region 2)	$\gamma\text{-FeOOH}$	220, 256, 314, 350, 382, 531, 652	-----	-----
	$\alpha\text{-FeOOH}$	301, 394, 415, 483, 552	254, 302, 394, 480, 555, 685	254, 302, 394, 479, 555, 685

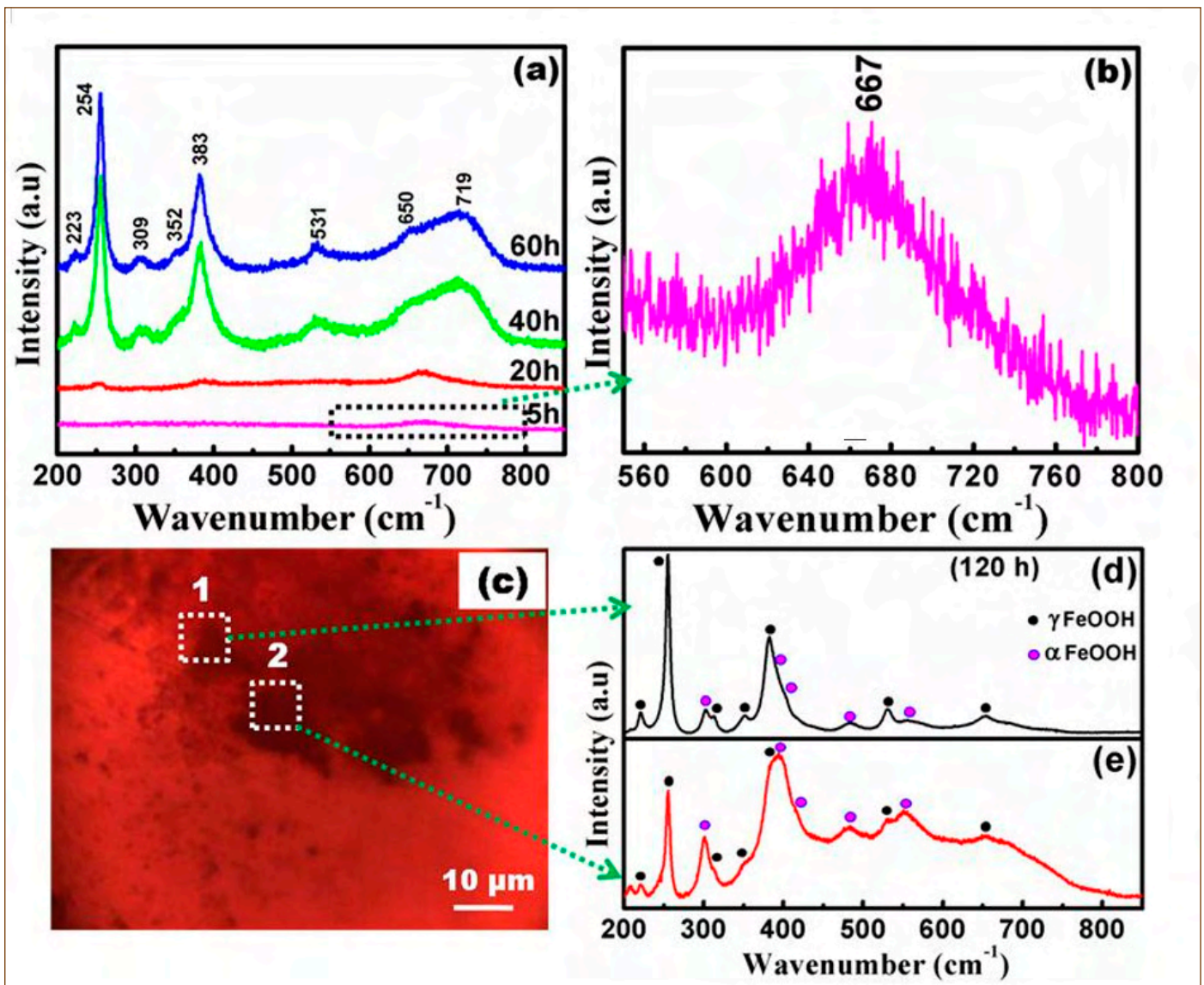


Figure 2: Photographs of bare modified 9Cr-1Mo specimens at different immersion times of 0, 5, 20, 40, 60 and 120 h, in acidic sulphate (a-f), neutral chloride (g-l), fresh water (m-r) and alkaline (s-x) solutions.

of the surface of the exposed specimen in concentrated chloride solution appear free from adherent corrosion deposits during entire exposure time. Further, the loosely bound rust clusters on the surface and solution, leave the freshly exposed surface to initiate more corrosion (more initiation sites) which could have resulted in the observed higher corrosion rate of 0.0827 mm/y in chloride solution. The corrosion rate was less (0.0155 mm/y) for the specimen immersed in the acidic sulphate solution containing sulphate anions, as compared to neutral chloride solution. The surface of the specimen exposed to the acidic sulphate solution, as shown in Figures 1a-f, revealed a uniform attack during the entire exposure times. Further, the rust deposits on the specimen surface were compact and uniformly covered. The in-situ laser Raman spectra revealed compact magnetite deposits beneath the Fe-oxy hydroxide layer, which resulted in a reduction in the

corrosion rate. A lower value of corrosion rate (0.0155 mm/y) was observed in fresh water due to the fact that fresh water contains less concentrated anions such as sulphate, chloride and carbonate etc., (9.5 mg l⁻¹, 30.3 mg l⁻¹, 65 mg l⁻¹ of SO₄²⁻, Cl⁻ and CO₃²⁻ respectively) which could have led to lower corrosive attack on the protective passive film (composed of Cr and Fe oxides) as shown in Figures 1m-r. However, crevice attack was observed on the bottom corner at initial exposure time of 5 h as shown in Figure 1n, which further intensified with time at the same location, leaving the other region on remaining surfaces un-affected. The corrosion rate of modified 9Cr-1Mo steel in acidic sulphate (pH~3), neutral chloride (pH~3), fresh water (pH~3) and alkaline (pH~10) media, at 120 h immersion time, are found to be 0.0155, 0.0827, 0.0043 and 0.0017 mm/y respectively.

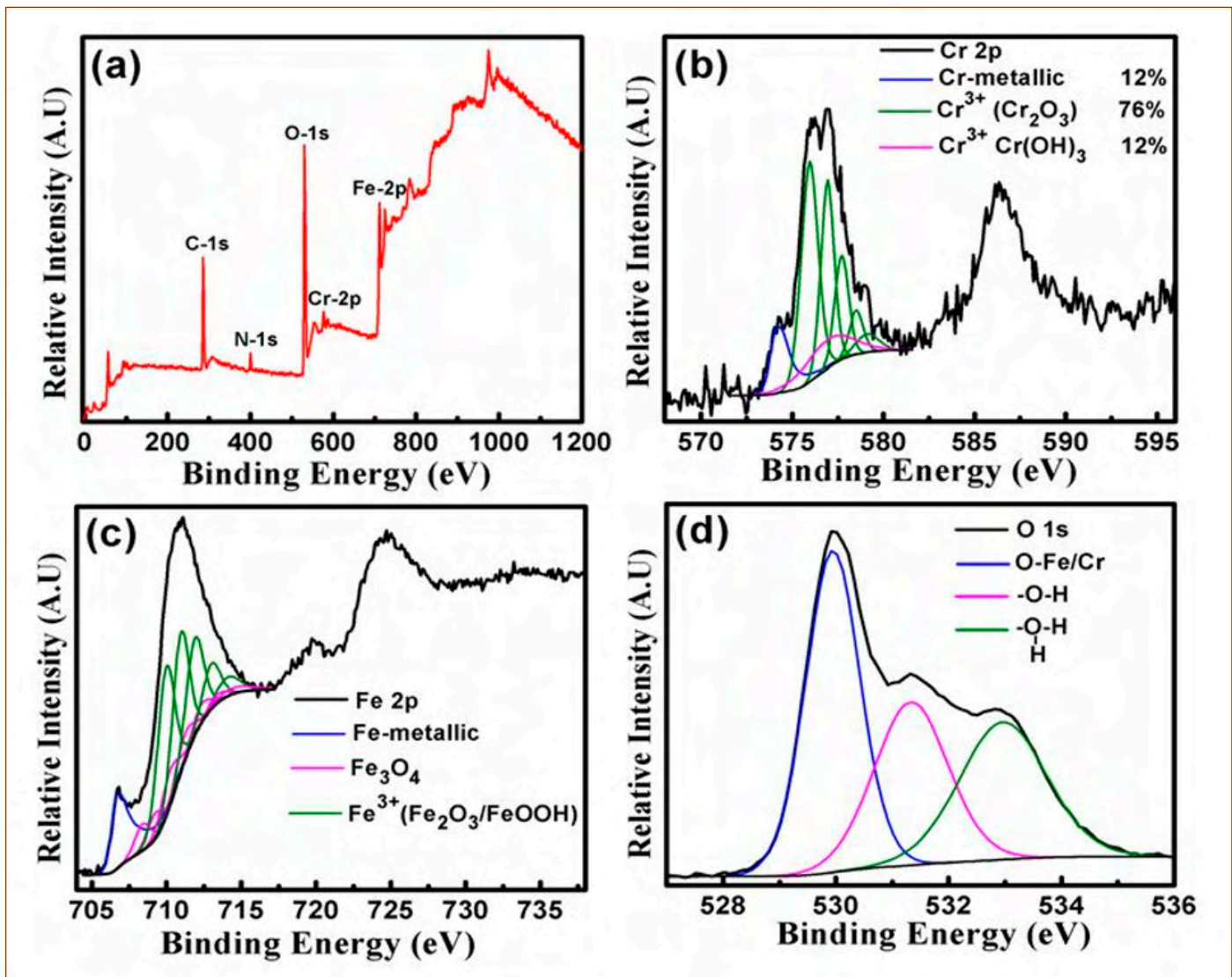


Figure 3: (a) XPS survey and de-convoluted high resolution spectra of (b) Cr $2p_{3/2}$; (c) Fe $2p_{3/2}$; (d) O 1s peaks on the passive film formed on modified 9Cr-1Mo steel specimen after exposure to alkaline solution for 120 h.

XPS analysis was performed on the modified 9Cr-1Mo steel surface exposed to alkaline solution for 120 h, to investigate the surface oxide composition within ~ 10 nm depth. The surface oxide film formed in alkaline solution is referred to as the passive film.

Apart from carbon peak, the XPS spectra of all other detected elements such as oxygen (O-1s), chromium (Cr-2p) and iron (Fe-2p) in the passive film after 120 h exposure in alkaline solution are given in Figure 3. The binding energy values of Cr and Fe with chemical states are shown in Table 2. In the passive film, the de-convoluted peaks in Cr $2p_{3/2}$ region (Figure 3b) showed two singlet peaks and multiplet peaks at the respective binding energies, corresponding to Cr existing in metallic (Cr^0) and +3 oxidation states (Cr_2O_3 , $\text{Cr}(\text{OH})_3$). Figure 3c shows the de-convoluted peaks of Fe $2p_{3/2}$ region. One singlet peak and two multiplet peaks were fitted at their binding energy values, which correspond to those of Fe in the

metallic state (Fe^0), and +2, +3 oxidation states of Fe_3O_4 , $\text{Fe}_2\text{O}_3/\text{FeOOH}$. The atomic concentration of oxide state of both Cr and Fe elements in the passive film of modified 9Cr-1Mo steel are shown in Table 2.

Element	Photo electron lines	Chemical state	Binding Energy (eV)	Atomic concentration
Cr	$2P_{3/2}$	Cr^{3+} (Cr_2O_3)	576	14
		$\text{Cr}^{3+} + \text{Cr}(\text{OH})_3$	577.3	2
Fe	$2P_{3/2}$	$\text{Fe}^{2+}/\text{Fe}^{3+}$ (Fe_3O_4)	708.2	20
		Fe^{3+} ($\text{Fe}_2\text{O}_3/\text{FeOOH}$)	710	64

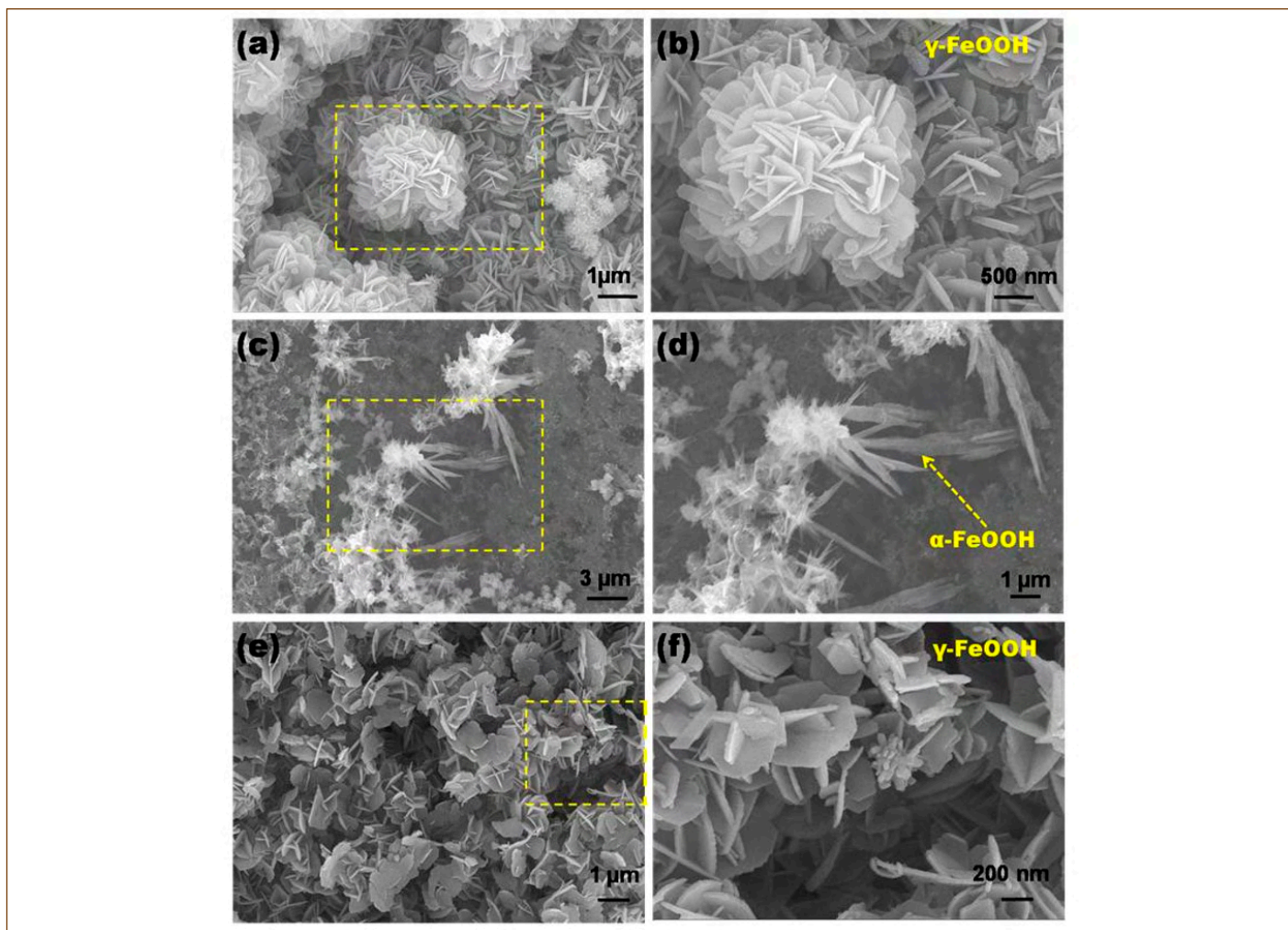


Figure 4: FE-SEM images of corroded surface of modified 9Cr-1Mo steel at different magnifications after exposure in acidic sulphate solution for 120 h. (a-b) Laminar lepidocrocite with flower like structures where the petals show vertical growth morphologies to the surface. (c-d) Acicular goethite formed on the laminar lepidocrocite structure. (e-f) Flower-petal shape lepidocrocite formed with serrated edges.

The ratio of oxide to metal (Cr and Fe) concentration was approximately 7:1 and 13:1, respectively, for Cr and Fe. Further, in the XPS survey spectrum (Figure 3a), the peaks corresponding to Mo was absent indicating that the passive films formed in alkaline solution is devoid of Mo.

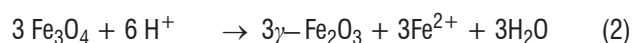
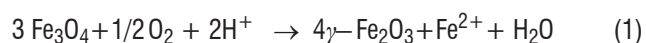
Figures 4a-f show the FE-SEM images on different areas of the rust layer formed on the modified 9Cr-1Mo steel specimen exposed in the acidic solution for 120 h. The surface showed a variety of crystalline morphologies such as globular petals (Figures 4a-b) comprising of flowery like structure, whisker/needle-shaped acicular formation (Figures 4c-d) and petals having serrated edges (Figures 4e-f). The petals shaped laminar morphologies correspond to γ -FeOOH phase and the acicular whiskers/needles seen clearly at magnified image (Figures 4d) at the periphery of the laminar structures correspond to goethite. It should be noted that the SEM image indicates lepidocrocite and goethite structures on the outermost surface of the rust layer, which was in good agreement

with our in-situ LRS results obtained at 120 h exposure. Further, the absence of magnetite morphologies (doughnut structure) in SEM images, which were seen in in-situ LRS spectra obtained at 5 and 20 h exposures, suggest that it was formed on the inner surface close to the base metal.

Based on the in-situ LRS results on initial corrosion products, the underlying corrosion mechanism of the modified 9Cr-1Mo steel in different aqueous solutions is elucidated and the results are compared with that of carbon steel to understand the role of alloying elements on corrosion of steel. In-situ LRS investigation on CS immersed in all the aqueous media revealed formation of green rust at all corrosion initiation sites, which was later transformed to lepidocrocite and magnetite. In case of modified 9Cr-1Mo steel, during the short exposure time upto 5 h, in all aqueous solutions, LRS has not detected any corrosion products, indicating feeble corrosion initiation. This could be due to the passive nature of the native films formed in air on the specimen surfaces. The initial

corrosion product identified was magnetite and then magnetite and γ -FeOOH after 5 h exposure. Studies show that magnetite is a transformed corrosion product of green rust in all pH conditions and is difficult to identify by in-situ Raman spectroscopy due to the rapid conversion of GR to γ -FeOOH phase. The identification of Fe_3O_4 and γ -FeOOH phases in LRS and the absence of green rust peaks after 5 h exposure, suggest that GR is rapidly transformed to Fe_3O_4 and γ -FeOOH.

In the acidic sulphate solution, due to the compact rust layer formation, made of both Fe_3O_4 and γ -FeOOH, minimal iron oxidation could have occurred, as compared to chloride concentrated solution where loosely bound rust clusters observed, which resulted in a lower corrosion rate in former. In addition to γ -FeOOH phase, an additional broad band at 719 cm^{-1} observed in the Raman spectrum after 40 and 60 h immersion is seen in acidic sulphate solution (Figure 2a) which correspond to γ - Fe_2O_3 . The transformation of Fe_3O_4 to γ - Fe_2O_3 can occur at a high temperature environment under various environmental conditions and the crystal structure of these two oxides is similar. The mechanism of transformation of magnetite into maghemite under oxic and anoxic conditions at ambient temperature in acidic solution was proposed by White et al. and the overall reaction can be written as



The appearance of the maghemite peaks along with lepidocrocite peaks after 40 and 60 h exposures, suggest that part of magnetite phase are transformed to maghemite by oxidation under the oxic condition. During 20 to 60 h exposure period, the major corrosion product formed on the modified 9Cr-1Mo steel surface was γ -FeOOH. At a longer immersion time of 120 h, the peaks of lepidocrocite and goethite phases are seen which suggest that lepidocrocite is partially transformed to goethite. Lepidocrocite occurs in soils in the anaerobic environment due to the formation of ferrous ions. However, lepidocrocite is transformed into goethite due to lower Gibbs free energy of formation of the latter. The mechanism of the reaction starts with the dissolution of lepidocrocite under the influence of high OH^- ion concentration according to



and re-precipitation lead to the formation of goethite.



The absence of goethite spectral peaks till 120 h immersion and its appearance after 120 h clearly indicate that the lepidocrocite phase is transformed to goethite phase. Further, it is known that alloying elements like chromium and manganese play an important role in the formation of corrosion products as they can hinder nucleation and growth of magnetite and promote stable goethite formation that reduces corrosion.

In-situ Raman spectroscopic technique was used to investigate the early corrosion products formed on modified 9Cr-1Mo steel specimens under naturally corroding conditions, in various aqueous solutions of different pH and anions. The key findings are: In acidic solution containing sulphate anions, uniform compact corrosion deposits are formed, whereas in chloride solution, non-compact loosely bound corrosion products formed at discrete sites via pitting. A crevice type corrosion attack was observed in fresh water. Fe_3O_4 and γ -FeOOH phases were the initially formed corrosion product in all media, except in alkaline solution. α -FeOOH is formed at longer exposure of 120 h. In alkaline solution, the specimen was un-reactive and remained passive during the entire exposure of 120 h. The ex-situ XPS analysis carried out after 120 h of exposure in alkaline medium confirmed higher the concentration of oxidized state of Cr and Fe in the passive film than the native film which shows the surface film thickness is more as compared to native film. XPS result confirmed that the corroded surfaces predominantly composed of Fe and Cr- oxy-hydroxide/oxide such as FeOOH, Fe_2O_3 , Cr_2O_3 , $\text{Cr}(\text{OH})_3$ in all exposure media. In chloride solution, Mn and Nb oxides were enriched on the surfaces, along with Cl^- ions in the rust layer, which suggests a chloride-induced corrosion attack on the surface. FE-SEM images show different types of laminar lepidocrocite and acicular goethite morphologies respectively, for γ -FeOOH and α -FeOOH phases. These morphologies could be well correlated with our in-situ LRS spectra at 120 h exposure time in all corrosive media except in alkaline solution, clearly revealing α -FeOOH nucleated from the γ -FeOOH phase. Thus the new insights obtained from this study are useful for a better understanding of early corrosion processes in different natural corroding conditions.

Young Researcher's Forum



Shri Supratim Mukherjee joined Metal Fuel and Pyroprocess Division (MFPD), Indira Gandhi Centre for Atomic Research as Scientific Officer-C in August 2018. He is from 61st batch (Chemistry) of BARC training School, Mumbai. He obtained his M.Sc. (Chemistry) degree in 2017 from Indian Institute of Technology, Kharagpur. At present, he is working in the area of metal fuel development and characterizations. He has published book chapter as well as peer-reviewed articles based on his work at MFPD.

In-house Development of High-Temperature Drop Calorimeter and Measurement of Enthalpy Increment of Magnesium Oxide

The principle aim of the thermodynamic study is the determination of partial molar quantities depending on concentration, temperature and pressure. Information on these calorimetric properties of various materials is required for conducting diversified physicochemical and thermal calculations. In nuclear industry knowledge of these thermodynamic properties of nuclear materials is essential for front-end (properties of oxide, carbide and metallic fuels) as well as back-end fuel cycle viz. immobilization of nuclear waste.

Drop calorimetry has long been the main experimental technique to measure thermodynamic properties such as enthalpy increment (ΔH) and to derive specific heat (C_p) of a substance. However nowadays, dynamic calorimeters became more widespread because of their high efficiency and less experimental time. At the same time drop calorimeter has number of advantages over dynamic calorimeters such as higher accuracy, sensitivity, wide temperature range of application, independent of type and geometric shape of samples and simple instrumentation. Therefore it continues to be the most reliable technique for determining heat content data. Thus, a high temperature (1273K), glove box adaptable, inert atmosphere drop calorimeter (Figure 1) is developed completely in-house and subsequently fabricated, installed at Metal Fuel Characterization and Process Section (MFCPS) of Material Chemistry and Material Fuel Cycle Group (MC&MFCG).



Figure 1: Photograph of in-house developed drop calorimeter.

1.0 Principle of Drop Calorimeter:

Principle of the drop calorimetry involves measurement of thermal effect as a result of instantaneously dropping a sample from a furnace to calorimeter. The samples are heated and thermally equilibrated in the furnace at a well-defined temperature of T_2 and dropped instantaneously into the receiving calorimeter maintained at 298K (T_1 , where $T_2 > T_1$) with negligible heat loss from the sample during dropping. Thermopile sensor placed inside the calorimeter measures the heat loss by the sample while cooling down from T_2 to T_1 (298K) in the form of voltage with respect to time. The measured heat effect is directly proportional

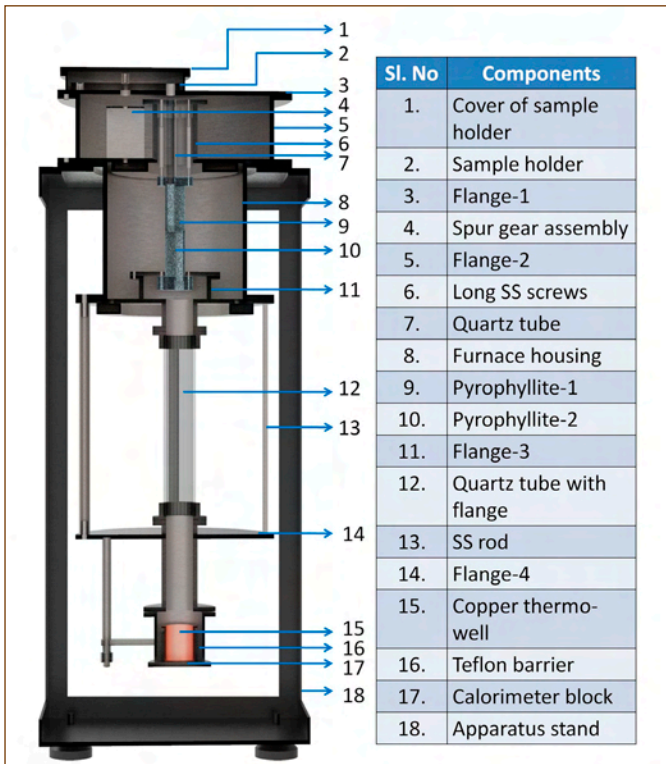


Figure 2: Cross-sectional diagram of drop calorimeter.



Figure 3: (a) Exploded diagram (b) Schematic diagram (c) Transparent view of drop calorimeter.

to ΔH and represented by area under the curve (A) of voltage-time curve and can be expressed as

$$[H_{T_2}^0 - H_{T_1}^0]_{sample} \propto A_{sample} \quad (1)$$

In all the cases this will be related to the specific heat of the material as expressed in equation 2.

$$\Delta H = \int_{T_1}^{T_2} C_p dT \quad (2)$$

By calibrating with a standard sample of known enthalpy increment value over the same temperature range, equation 1 can be expressed as

$$[H_{T_2}^0 - H_{T_1}^0]_{sample} = \frac{A_{sample}}{A_{standard}} \times [H_{T_2}^0 - H_{T_1}^0]_{standard} \quad (3)$$

Heat capacity of the sample can be calculated using equation 2 and 3. Higher accuracy can be achieved by nullification of additional instrumental error.

2.0 Description of the Drop Calorimeter:

In Figure 2, a cross-sectional diagram of the apparatus in the current configuration is presented. The apparatus comprises five main parts: auto-sampler, furnace block, sample dropping assembly, calorimetric receiving block and instrumentation. Detailed arrangements of all the components of the apparatus are represented in 3D design in Figure 3. All components are fixed

together with gasket and o-rings for leak-tight arrangement which enables it to operate in desired experimental atmosphere (inert, HP-Ar and air). Leak tightness was checked and ensured by He-leak testing. Glove box adaptability of the apparatus is achieved by modified design as well as separating other instrumentation part from the main system. The brief description of all the components is as follows.

2.1 Auto-sampler:

This part consists of a sample holder with four slots and top flange. Sample holder can rotate on top flange by controlled rotation mechanism guided by stepper motor 1. This rotation mechanism controls loading of one sample at a time into the hot zone of pre-heated furnace. This auto sampling mechanism of four samples (two samples and two standards) not only enhances efficiency and ease of usage by reducing experimental time but also provides same experimental conditions such as inert atmosphere for samples and standards.

2.2. Furnace block:

This part consists of a platinum furnace, flange-2, pyrophyllite-1, pyrophyllite-2, furnace housing and flange 3. A high temperature (1373K) vertical furnace of inner diameter 25mm with platinum as heating element (resistance of 3.4ohm) is used here. The temperature of the furnace is kept constant to within $\pm 0.1K$ by a Eurotherm temperature controller with a K-type thermocouple

temperature sensor. All the necessary connectors are taken to the controller through feedthroughs to attain leak tightness. Controller also has a software interface (Figure 4) which is connected to computer for manual inputs. Pyrophyllite-1 and pyrophyllite-2 is placed inside the furnace and pyrophyllite-1 receives the sample from the auto-sampler through an extended quartz tube. The sample is allowed to heat, thermally equilibrated at desired temperature (T_2) inside this pyrophyllite-1. A spur gear guided rotation mechanism causes dropping of the sample from pyrophyllite-1.

2.3. Calorimetric receiving block:

The sample directly drops in to a copper thermo-well inside the calorimeter block, which is maintained at 298K by cooled water jacket. All the heat loss from the sample is gained by the copper thermo-well and measured precisely by thermopile sensor.

2.4. Calorimeter data acquisition system:

It consists of a thermopile sensor placed under the thermo-well, Keithley meter, PC interface software and PC. Thermopile sensor (TEC-12706) generates mV range signal corresponding to the change in temperature of the thermo-well due to dropping of the heated sample from the furnace. This is fed to a high impedance multi-meter ($6\frac{1}{2}$ digit) of high accuracy and precision for

measurement and transferring signal to computer via computer interface software. The interface software was developed in-house and described in IGC Report 319 (2013). Figure 5 shows the typical recorded signal after dropping standard alumina sample heated at 723 K. The heat energy released by the standard alumina sample for cooling down from 723K to 298K is represented as area under the curve. Hence enthalpy increment (ΔH) of an unknown sample can be determined using equation 1 and 3 respectively and specific heat capacity value could be calculated.

3.0 Precision of the drop calorimeter:

To evaluate the precision of the apparatus standard alumina pellet supplied by NBS, USA (mass 0.094g) was heated to 723 K dropped subsequently to calorimeter block and the experiment is repeated for three times. Standard deviation is found to be within 0.056. (Table 1)

Table 1: Repeatability of the generated data			
Expt No.	Area	Standard deviation	Error margin
1.	5.820	0.0451	5.8781 \pm 0.0511 95%confidence
2.	5.884		
3.	5.930		

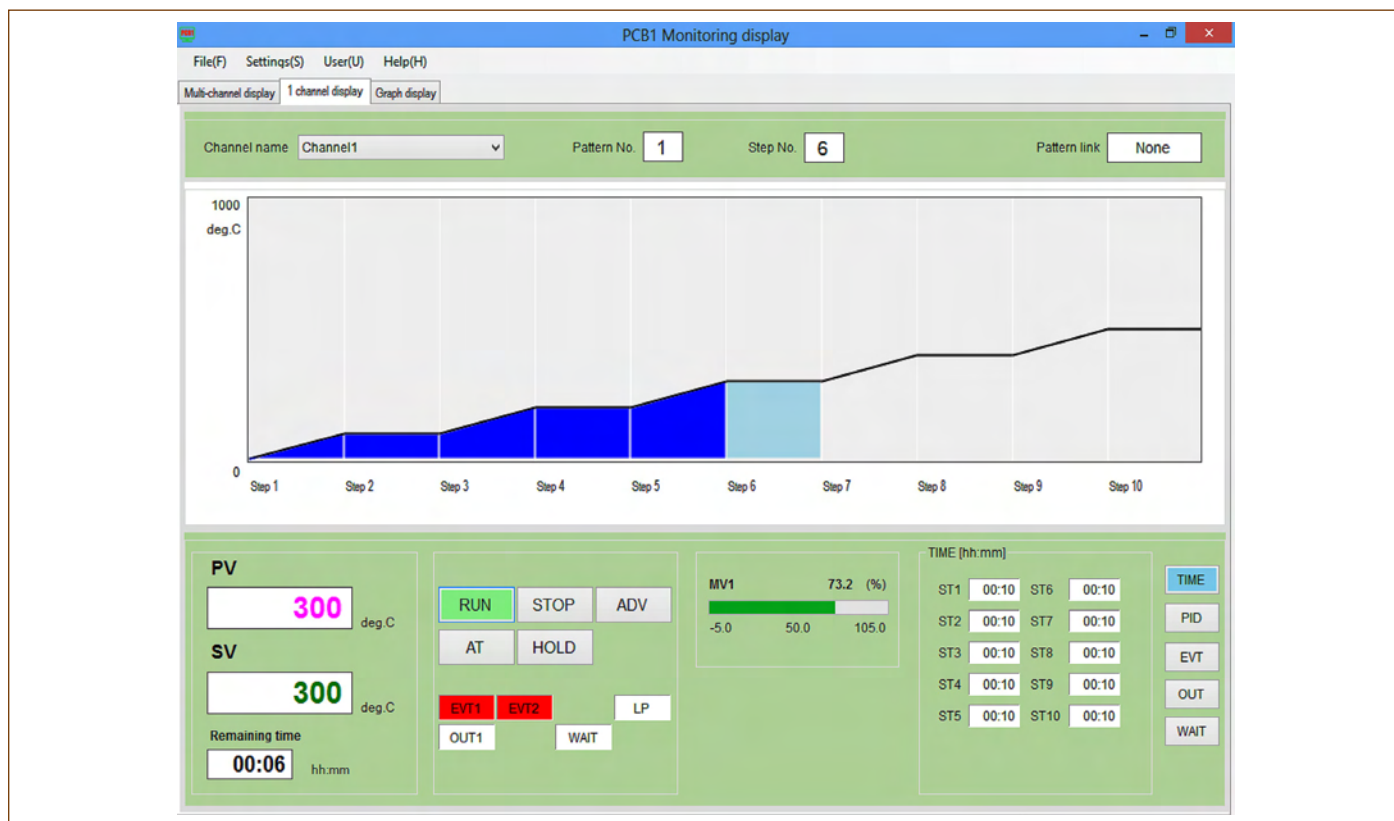


Figure 4: Software interface of furnace controller.

4.0 Measurement of Enthalpy increments of MgO for evaluation of the accuracy:

To determine accuracy of developed drop calorimeter, enthalpy increment data of MgO (single crystal, procured from Crystec, USA) of mass 0.1048 g is chosen as sample and enthalpy increment is measured in the temperature range of 323K to 823K using standard alumina as reference. All the data was fitted to the equation 4 using non-linear least square fitting program.

$$H_T^0 - H_{298}^0 = a + bT + cT^2 + d/T \quad (4)$$

Table 2: Molar Enthalpy data of MgO

Temperature (K)	$H_T^0 - H_{298}^0$ (J/mol)	
	Measured	Literature (Knacke)
298	-	0.0
373	2912.9	3043.8
473	7393.9	7419.5
573	11844.2	12069.3
673	16764.9	16883.7
773	21858.1	21810.4
873	26702.4	26822.8

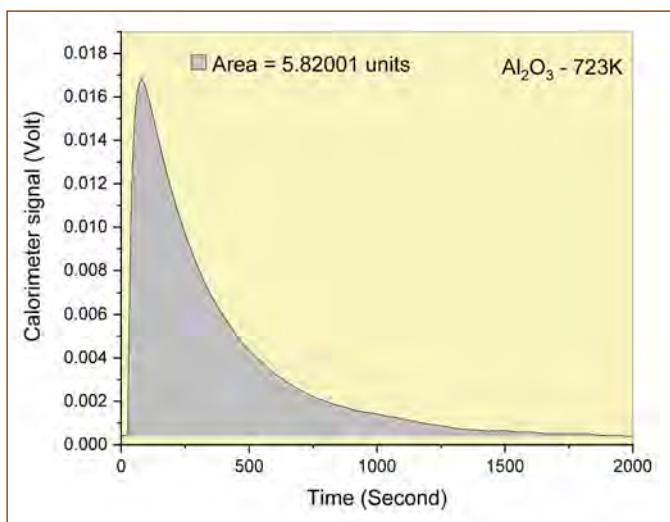


Figure 5: Voltage output vs time plot of standard alumina heated up to 723K.

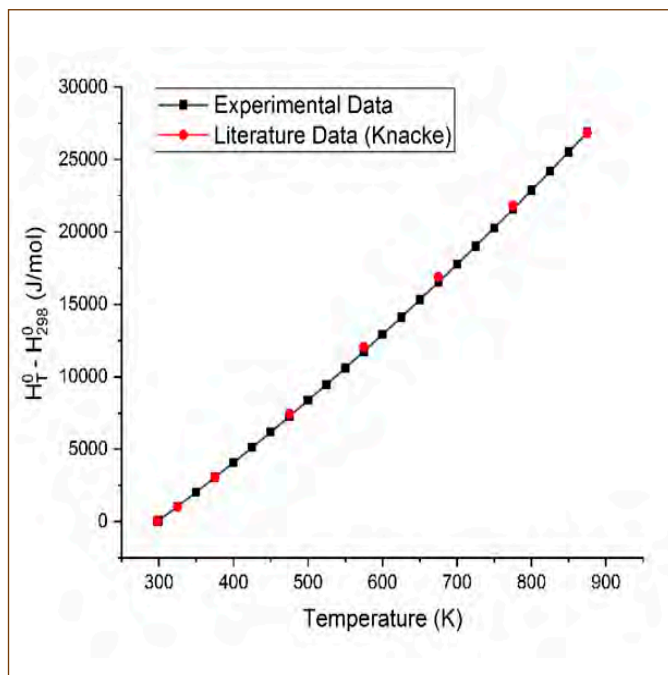


Figure 6: The enthalpy increment data for MgO measured using the drop calorimeter.

All measured data is enumerated in Table 2 and plotted against literature values reported by Knacke et al. (O. Knacke, Thermophysical properties of inorganic substances, 2nd ed. Berlin: Springer-Verlag; 1991) in figure 6. The mean error in the enthalpy increment values found to be within $\pm 1.1\%$.

To conclude, an isoperibol type glove box adaptable drop calorimeter instrument with high precision and accuracy is developed completely in-house. The equipment is capable of measuring enthalpy increment of solid samples from 323K to 1273K in air or inert ambient. This will be useful to measure thermal properties of nuclear materials. Moreover hitherto most of thermal analysis instruments viz. Drop calorimeter, Differential Scanning Calorimetry (DSC) and Differential Thermal Analysis (DTA), etc. are still procured from overseas. This indigenous development can be accorded as a first step towards self-reliance in the development of glove box adaptable drop calorimeter in the temperature range of 323K to 1273K.

News and Events

Webinar - International Conference on Light Matter Interaction (ICLMIN – 2021)

May 19-21, 2021



The webinar was attended by more than 800 leading scientists and student all over the world across six sub-continent of Africa, Asia, Australia, Europe, North and South America.

International Conference on Light Matter Interaction (ICLMIN – 2021) was organized by Indira Gandhi Centre for Atomic Research (IGCAR), Kalpakkam during May 19-21, 2021 in online mode [<https://sites.google.com/view/iclmin2021/home>; <https://iclmin2021.in/index.html>].

The conference focused on Light-Matter Interaction and its study using Optical Spectroscopy along with their applications in material sciences encompassing physical, and chemical sciences. The conference was inaugurated by Dr. A. K. Bhaduri, Director IGCAR with welcome address by both Dr. Shaju Albert, Director MSG and Dr. M. Kamruddin, Associate director, ANG. Chief Guest Prof. Chandrabhhas Narayana, Director, Rajiv Gandhi Centre for Biotechnology (RGCB), Trivandrum delivered the plenary lecture on "Application of Surface Enhanced Raman Spectroscopy for studying Bio-molecular interactions" for the opening session.

The conference focused on the utilization of conventional as well as advanced optical spectroscopy on novel low dimensional materials, along with specific sessions on phase transformations under extreme conditions, and single quantum emission. Localized techniques namely near-field scanning optical microscopy (NSOM) assisted, and surface and tip enhanced Raman spectroscopy (SERS and TERS) are another area of major interest. The webinar was attended by more than 800 leading scientists and student all over the world across six sub-continent of Africa, Asia, Australia, Europe, North and South America. Indian participants were spread all over the country. The scientific deliberations were conducted in eight technical sessions with invited and contributory presentations. The conference presented an opportunity for young researchers to interact with leading experts in the specialized field of research. There were 13 foreign speakers spreading over five sub-continent and 18 Indian speakers from IITs, National Universities and Research Institutes.

Conference was attended by 800 participants and was well appreciated by all.

Media Coverage: <https://pib.gov.in/PressReleasePage.aspx?PRID=1721373> (Please use google translator)

<https://www.chennaiacitynews.net/news/tamilnadu/international-conference-on-light-matter-interaction-iclmin-2021/>

<https://kalaipoonga.net/business/international-conference-on-light-matter-interaction-iclmin-2021/>

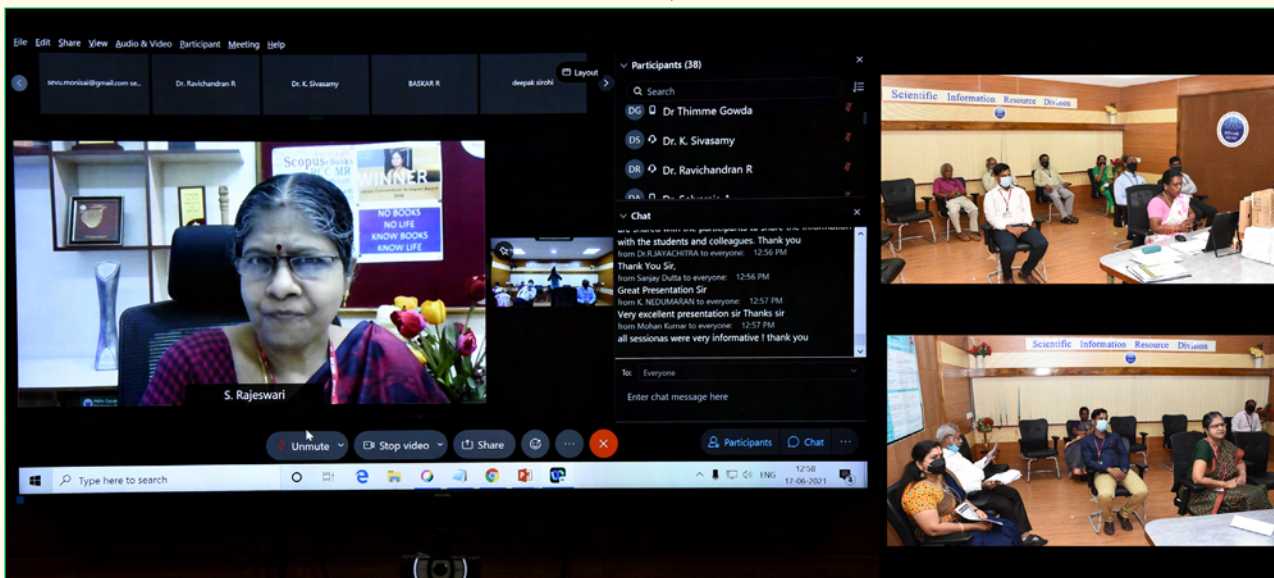
Reported by

Dr. Sandip Dhara, Materials Science Group

News and Events

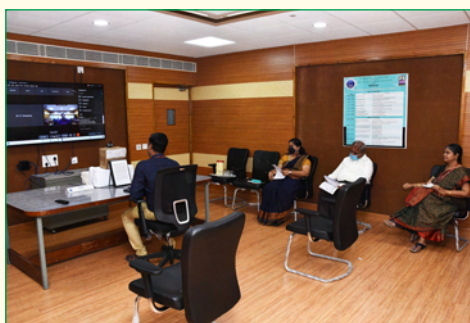
Webinar on Emerging Trends in Digital Research Library

June 16-17, 2021

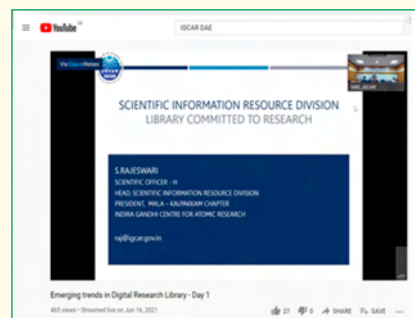


Presidential Address by Smt. S. Rajeswari, Head, SIRD

Scientific Information Resource Division (SIRD) in association with the Madras Library association, Kalpakkam Chapter organized a two-day webinar on Emerging Trends in Digital Research Library during June 16-17, 2021. There were more than 300 participants for the webinar. The webinar was live streamed through Webex platform and official YouTube of IGCAR. The registered participants joined through YouTube. The speakers and dignitaries were on Webex platform. Shri.E.Soundararajan, Head, DRTS, SIRD welcomed the delegates of the webinar. The inaugural address was given by Dr. B. Venkatraman, Distinguished Scientist and Director SQRMG. Smt. S. Rajeswari, Head, SIRD delivered the presidential address. The webinar focused on the emerging technologies and trends for research digital library and highlighted the impact of library in R&D output of institutions. There were technical talks by eminent speakers from SIRD, Pondicherry University, Madras Library Association and NITTR, Chennai. The presentations ranged from emerging trends in digital library infrastructure, research and publication ethics, research data management and analysis through institutional repository and scientometrics to name a few. All the sessions were quite interactive. Participation Certificates were mailed to the registered participants in digital format. The YouTube link for the webinar is <https://www.youtube.com/watch?v=xAWGqnZPIMY> and <https://www.youtube.com/watch?v=3s5DLH6NL8w> for day 1 and day 2 respectively.



Indira Gandhi Centre for Atomic Research (IGCAR)		
Scientific Information Resource Division (SIRD)		
in association with		
Madras Library Association Kalpakkam chapter (MALA-KC)		
organizes		
Webinar		
on		
Emerging Trends in Digital Research Library		
Day-1 (16-06-2021)		
Timing	Topic	Speaker
10:30 - 10:35	Welcome Address	Dr. B. Venkatraman Secretary, MALA-KC
10:35 - 10:40	Invocation Address	Dr. E. Venkatarajan, Distinguished Scientist Director, SIRD, IGCAR
10:40 - 11:10	Presidential Address	Smt. S. Rajeswari President, MALA-KC and Head, SIRD, IGCAR
11:10 - 11:20	Special Address-1	Dr. E. Soundararajan President, Madras Library Association
11:20 - 11:30	Special Address-2	Dr. E. Venkatarajan Secretary, Madras Library Association
11:30 - 11:40	A journey of scientist with Publications	Dr. S. S. Srinivasan Head, LIS, SIRD, IGCAR
11:40 - 12:00	Emerging trends in Digital library infrastructure	Dr. E. Soundararajan Head, LIS, SIRD, IGCAR



Reported by
Smt. S. Rajeswari, Head, SIRD

DAE Awards



Department of Atomic Energy has instituted annual awards for excellence in Science, Engineering and Technology in order to identify best performers in the area of Research, Technology Development and Engineering in the constituent units (other than Public Sector Undertakings and Aided Institutions). The Young Applied Scientist, Young Engineer, Young Technologist, Homi Bhabha Science and Technology Award and Scientific and Technical Excellence Award fall under this category. Group Achievement awards for recognition of major achievements by groups have also been instituted. Life-time Achievement Award is awarded to one who has made significant impact on the DAE's programmes. They are the icons for young scientists and engineers to emulate. The awards consist of a memento, citation and cash prize.

The recipients of the Awards from IGCAR for the year 2019 were:

DAE Scientific and Technical Excellence Award	: 1. Shri Rakesh Kumar Mourya, SO/F, SE&HD, RDTG 2. Shri Utpal Borah, SO/G, MDTD, MMG
Young Scientist Award	: Dr. G. Sainath, SO/E, MDTD, MMG
Young Engineer Award	: 1. Shri P. Lijukrishnan, SO/E, ETHD, RDTG 2. Shri E. Vetrivendan, CSTD, MMG
Meritorious Service Award	: Shri S. Palavesamuthu, GM, Canteen, Admin
Meritorious Technical Support Award	: 1. Shri I. Amir, Abhas, FM/C, ROD, RFG 2. Smt. M. Padalakshmi, PIED, MMG

Group Achievement Awards:

"Life extension of FBTR Through an integrated Strategy"

Dr. P. Parameswaran (Group Leader)

Dr. S. Raju, Dr. V. Thomas Paul, Smt. T. Ezhilarasi, Shri R. Thirumurugesan, Shri A. K. Panda, Dr. S. Murugesan, Smt. M. Jyothi, Dr. C. Sudha, Dr. Harapasanna Tripathy, Shri R. Sundar, Smt. M. Padalakshmi, Dr. R. Divakar, Dr. V. Karthik, Shri C. N. Venkiteswaran, Shri A. Vijayaragavan, Dr. C. Padmaprabhu, Shri V. Anandaraj, Shri V. V. Jayaraj, Shri Ran Vijay Kumar, Shri Ashish Kolhatkar, Shri M. Sakthivel, Shri Bhabani Sankar Dash, Shri L. Pandian, Smt. S. Gomathi, Shri Rabindra Nayak, Shri Panchanan Patra, Shri V. Murugan, Shri S. Anguraj, Shri S. Manimaran, Shri P. Loganathan, Shri V. Rajendran,

Shri B. S. Ramesh Babu, Shri K. Dinesh, Shri .S. Rama Rao, Shri G. Bhaskaran, Shri Shobit Verma, Shri R. Athisankaran, Shri G. Raghukumar, Smt. E. Radha , Smt. Neethu Hanna Stephen, Shri V. Velu, Shri V. Rajkumar, Shri P. K. Chaurasia, Shri M. Muthuganesh, Shri R. Ravikumar, Shri Rajesh Saxena, Shri Adish Haridas, Dr. D. Venkata Subramanian, Shri Rajeev Ranjan Prasad, Dr. D. Sunil Kumar, Shri R. Ramesh, Dr. S. Murugan, Shri G. Ramesh, , Smt. Alka kumari, Shri P. Ramesh, Dr. K. Chandran, Mrs. M. Lavanya, Dr. R. Raja Madhavan, , Dr. R. Sudha, Dr. Anthonysamy

Group Achievement Awards:

"Development of welding and Inspection Procedures for Disimilar Metal Weld Joint between 10Cr Steel & Alloy 617M Welded Rotor for Advanced Ultra Super Critical (AUSC) Thermal"

Dr. Shaju K. Albert (Group Leader)

Dr. Arun Kumar Bhaduri, Dr Harish Chandra Dey, Dr. Anish Kumar, Shri Utpal Borah, Dr. K. V. Rajkumar, Shri S. Pongseenuvasan, Shri Arvinth Davinci Shri M. Arul, Shri D. Manokaran, Dr. C. Ravishankar from MMG. Shri S. Murugan, Shri V. Rajandran, Shri T. Saravanan, Shri C. Palani, Shri D. Mohan, Shri S. P. Jaisankar, Shri E. Gothandan, Shri B. Sathish Kumar, Shri B. Muhammed Shijas, Shri A. Ramanathan, Shri R. Manikandan, Shri S. Surendra Kumar, Shri E. Damodaran, Shri K. Punniyakotti, Shri Bhagaban Mohanty, Shri P. Karuppasamy, Shri V. Kodairasan, Shri A. Gunasekaran from ESG. Shri Navtresh Bajpai, Shri K. Krishna Chaitanya, Shri P. Azhagesan, Shri P. Narayana Rao, Shri R. Rajesh from SQ&RMG

Group Achievement Awards:

"Development of Robotic vehicle and Remotely Operated Devices for the Visual Inspection of Fast Reactor Fuel Reprocessing Facilities"

Shri C. Rajagopalan (Group Leader)

Dr. S. Murugan, Dr. Purna Chandra Rao B, Shri Joseph Winston, Shri R. Chellapandian, Shri G. Senthil Kumaran, Shri Saji Jacob George, Shri V. Rakesh, Shri Ashutosh Pratap Singh, Shri M. Murali, Shri K. Dhanapal, Shri Jobby C Johnson, Shri D. Ganesan, Smt Shanthi Rajendran, Smt. S. Saravana Priya from RDTG. Shri A. K. Sasi, Shri Shekhar Kumar, Shri M.S. Gopi Krishna, Shri Surajit Halder, Shri P. Varadharajan, Shri Abdul Muqtadir, Shri D. C. Thomson from RpG. Shri G. Ramesh from SQ&RMG

Group Achievement Awards:

"Indigenous Design, Development and Implementation of Electronics Security Systems and Computer Based Security Automation for DAE Kalpakkam Complex"

Shri G. Prabhakara Rao (Group Leader)

Shri P. Arumugam, Shri S. Krishnan, Shri M. Vincent, Shri Gyanendra Prasad, Shri S. Lakshmi Prasad, Shri Satya Rajesh Medidi, Shri I. Gowtham, Shri T. Sathishkumar, Shri M. Raja Sekhar, Shri P. Balaji, Shri J. Immanuel from EIG

Online Events

- Webinar on “Corrosion Science and Technology COST 2021” was organized by CSTD, MMG, IGCAR in association with IIM Kalpakkam Chapter on May 12, 2021.
- Online Training programme on Reservation in services held on June 23,2021, Admin Section
- Online Training programme on Stress Management, Admin Section, June 24,2021
- Online Training programme on National Pension Scheme, Admin Section, June 25,2021
- Online Training programme on Office Procedure and Record Management, Admin Section, June 28-29,2021
- Online Training programme on CCS pension rules (1972), Admin Section, June 30,2021

Awards and Honours

Prof. Placid Rodriguez Memorial Lecture (2020) award to **Dr. Harish Chandra Dey**, MMG by IIW India
“Development of Welding Procedures for Critical Applications in Nuclear and Fossil Power Plants”
National Welding Seminar 2020-21, April 8-10, 2021, Baroda

Best Paper/Poster Awards

Best Paper Award

S. C. Vanithakumari, Geetisubhra Jena, Sofia Solomon, C. Thinaharan, R.P. George and John Philip
“Fabrication of superhydrophobic titanium surfaces with superior antibacterial properties using graphene oxide and silanized silica nanoparticles”
Surface and Coatings Technology 400 (2020) 126074

Manali Nandy, B. B. Lahiri and John Philip
“Visual detection of defects in carbon steel using magnetic nanoemulsions effect of stabilizing moieties on the defect detection sensitivity”
Sens. Actuators A, 314 (2020) 112220

Nanda Gopala Krishna, R. P. George and John Philip
“Anomalous enhancement of corrosion resistance and antibacterial property of commercially pure Titanium (CP-Ti) with nanoscale rutile titania film”
Corrosion Science 172 (2020) 108678

Bio-diversity @ DAE Campus, Kalpakkam

Rose-ringed Parakeets



© SIRD, IGCAR

Rose-ringed Parakeets are long-tailed parrots commonly seen everywhere in Kalpakkam. It has a grassy green feather with a long graduated tail and a red bill. In the photograph, the male is distinguished by a black chin stripe joining with a pink hint collar, while the female lacks the chin stripes and the collar is all green in color.

Editorial Committee Members: Ms. S. Rajeswari, Dr. V. S. Srinivasan, Dr. John Philip, Dr. T. R. Ravindran, Dr. C. V. S. Brahmananda Rao, Shri A. Suriyanarayanan, Shri M. S. Bhagat, Shri G. Venkat Kishore, Dr. Girija Suresh, Shri M. Rajendra Kumar, Shri S. Kishore, Shri Biswanath Sen, Dr. N. Desigan, Shri Gaddam Pentaiah and Shri K. Varathan